

# On the anisotropic density distribution on large scales

Péter Pápai<sup>1</sup>, Ravi K. Sheth<sup>1,2</sup>

<sup>1</sup>CEI Fellow, The Abdus Salam International Center for Theoretical Physics, Strada Costiera, 11, Trieste 34151, Italy

<sup>2</sup>Center for Particle Cosmology, University of Pennsylvania, 209 S. 33rd St., Philadelphia, PA 19104, USA

10 July 2012

## ABSTRACT

We derive a formula for the anisotropic density distribution around haloes and voids on large scales. Our model assumes that the orientation of non-linear structures is strongly correlated with the Lagrangian shear, and gives a qualitative understanding of the recent detection of an enhanced clustering signal along the major axis of haloes. We also show that the measured amplitude is inconsistent with a model in which the alignment is produced by the initial inertia rather than shear tensor.

**Key words:** large-scale structure of Universe

## 1 INTRODUCTION

The clustering of matter at late times provides important constraints on cosmological models. Our understanding of the signal is best on large scales, where it can be described by perturbation theory well (see e.g. Peebles 1980). E.g., the Baryonic Acoustic Oscillations in the power spectrum (BAO), which appear as a spike in the two-point correlation function, lie in this regime (see e.g. Eisenstein 2005). In addition to the simple correlation function, there are other ways to extract information from the matter distribution. In redshift-space distorted measurements, the two-point correlation function is anisotropic (see e.g. Kaiser 1987 or the recent work of Schlagenhauser et al. 2012), and this anisotropy can be used to constrain cosmological parameters. However, certain real-space measures of clustering are also expected to be anisotropic. E.g., galaxy clusters are typically triaxial, and this triaxiality has long been known to align with the surrounding large scale structure (e.g., Smargon et al. 2012, and references therein). On smaller mass scales, galaxy spins are also known to align with the environment (e.g., Jones et al. 2010; Lee & Pen 2001).

Recently, Faltenbacher et al. (2012) showed that, in their numerical simulations of hierarchical gravitational clustering, the cross-correlation function between haloes and the surrounding mass was anisotropic: this correlation between halo shapes and large scale structure extended even to the large scales relevant to BAO studies, and affected the zero-crossing of the correlation function. This motivates our work, which attempts to model this anisotropy.

Our model, which is described in Section 2, is based on the assumption that halo shapes (Lee et al. 2005; Rossi et al. 2011) and orientations (Lee & Pen 2001) at late times are correlated with the properties of the initial Lagrangian field from which they formed. This is a fundamental ingredient in models where haloes form from a triaxial

collapse (Bond & Myers 1996; Sheth et al. 2001). In such models, the Lagrangian deformation or shear tensor plays a key role, as its eigenvalues can be used to distinguish between haloes, filaments, walls and voids. We illustrate our model for the two extreme cases: haloes and voids. A final section discusses potential applications and extensions of our work.

Although our analysis is general, when we illustrate our results, we will assume a  $\Lambda$ CDM model with  $h = 0.73$ ,  $\Omega_{\text{cdm}} = 0.215$ ,  $\Omega_{\text{bar}} = 0.035$ ,  $\Omega_{\Lambda} = 0.75$ , and  $\sigma_8 = 0.9$ . These values facilitate comparison with the simulations of Faltenbacher et al. (2012).

## 2 ANISOTROPIC DENSITY DISTRIBUTION AROUND HALOES

Despite the fact that haloes are highly non-linear objects, their formation encodes information about the initial (Lagrangian) fields from which they formed (e.g., Press & Schechter 1974; Sheth et al. 2001), so, for example, one expects the shape, spatial orientation and spin of a halo to be correlated with the initial tidal field (e.g., Lee & Pen 2001; Rossi et al. 2011).

### 2.1 The shear

The initial tidal field or shear tensor is defined as

$$\xi_{ij}(\mathbf{q}) \equiv \frac{1}{\sigma_0} \frac{\partial^2 \Phi(\mathbf{q})}{\partial q_i \partial q_j}, \quad \text{where } \Delta \Phi(\mathbf{q}) \equiv \delta(\mathbf{q}), \quad (1)$$

where  $\mathbf{q}$  is the Lagrangian spatial coordinate,  $\Phi$  is the Lagrangian potential at  $\mathbf{q}$ , and  $\sigma_0^2$  is the variance of the Lagrangian density  $\delta$  smoothed on scale  $R$ . This variance de-

pends on the power spectrum  $P(k)$  and the smoothing filter:

$$\sigma_j^2 = \int dk k^2 k^{2j} P(k) W_R^2(k). \quad (2)$$

For the  $\Lambda$ CDM parameters given earlier, we obtain the linear theory  $P(k)$  from CAMB (Lewis et al. 2000). The resulting  $\sigma_j$  decreases monotonically as  $R$  increases. As a result, in the excursion set description of haloes or voids (Bond et al. 1991; Sheth & Tormen 2002),  $\sigma_0$  decreases as the halo mass or void radius increases. This will be important when we wish to relate our results to the halo-based measurements in simulations.

In what follows, we would like to estimate the anisotropy in the correlation between the density distribution at one position given that the shear at another position (which we will take to be the origin) satisfies some set of constraints. That is to say, we are interested in

$$\begin{aligned} \langle \delta(\mathbf{r}) | \Xi \rangle &= \frac{\int_{\Xi} d\xi p(\xi) \int d\mathbf{r} \delta(\mathbf{r}) p(\delta(\mathbf{r}) | \xi)}{\int_{\Xi} d\xi p(\xi)}, \\ &= \frac{\int_{\Xi} d\xi p(\xi) \langle \delta(\mathbf{r}) | \xi \rangle}{\int_{\Xi} d\xi p(\xi)} = \frac{\int_{\Xi} d\xi p(\xi) \langle \delta(\mathbf{r}) | \xi \rangle}{P(\Xi)}, \end{aligned} \quad (3)$$

where  $\xi = (\xi_{11}, \xi_{22}, \xi_{33}, \xi_{12}, \xi_{23}, \xi_{13})$  is a vector made from the components of the shear tensor and, for simplicity, we omit the distance argument  $\mathbf{r}$  if the quantity in question is taken at the origin: e.g.  $\xi \equiv \xi(0)$ . In the expression above,  $\Xi$  is the region in  $\xi$ -space where the conditions on the shear field (associated with halo or void formation) are satisfied; we use  $P(\Xi)$  to denote the integral over this region. For Gaussian initial conditions,  $p(\xi)$  is a multivariate Gaussian.

## 2.2 Average of $\delta(\mathbf{r})$ with conditions on the shear

The Gaussianity of  $p(\delta(\mathbf{r}) | \xi)$  means that

$$\langle \delta(\mathbf{r}) | \xi \rangle = \langle \delta(\mathbf{r}) \otimes \xi \rangle \langle \xi \otimes \xi \rangle^{-1} \xi \quad (4)$$

where neither  $\langle \delta(\mathbf{r}) \otimes \xi \rangle$  nor  $\langle \xi \otimes \xi \rangle^{-1}$  depend on  $\xi$ . Therefore

$$\langle \delta(\mathbf{r}) | \Xi \rangle = \langle \delta(\mathbf{r}) \otimes \xi \rangle \langle \xi \otimes \xi \rangle^{-1} \langle \xi | \Xi \rangle. \quad (5)$$

The first two terms depend only on the correlations between  $\delta$  at one position and the shear tensor  $\xi$  at another. Such correlations have been computed before Doroshkevich (1970); Bardeen et al. (1986); Desjacques (2008). We used the form for  $\langle \xi_{ij}(r) \xi_{kl} \rangle$  that is given in the appendix of Desjacques (2008). Although this expression can be worked out exactly for the  $6 \times 6$  covariance matrix associated with  $\xi$ , it is simpler to work in the coordinate system which is aligned with the principal axes of the shear tensor. In this case, we find that

$$\langle \xi \otimes \xi \rangle^{-1} = \begin{pmatrix} 6 & -3/2 & -3/2 \\ -3/2 & 6 & -3/2 \\ -3/2 & -3/2 & 6 \end{pmatrix}. \quad (6)$$

Similarly, using the fact that  $\delta/\sigma_0 \equiv \sum_i \xi_{ii}$ , where  $\sigma_0$  was defined in equation (1), we find

$$\langle \delta(\mathbf{r}) \xi_{ij} \rangle / \sigma_0 = -\Delta_2(r) \hat{r}_i \hat{r}_j + \frac{1}{3} (\Delta_0(r) + \Delta_2(r)) \delta_{ij}, \quad (7)$$

with  $\hat{r}$  being a unit vector and

$$\Delta_n(r) \equiv \frac{1}{2\pi^2 \sigma_0^2} \int dk k^2 j_n(rk) W_R(k) P(k), \quad (8)$$

where  $j_n$  is a spherical Bessel function, and  $W_R$  is the window function of scale  $R$  over which the shear is smoothed.

Since

$$\sigma_0^2 \Delta_2(r) \equiv \bar{\xi}_{2pt}(r) - \xi_{2pt}(r) \quad (9)$$

where  $\xi_{2pt}(r) = \sigma_0^2 \Delta_0(r)$  is the usual angle-averaged two-point correlation function, and

$$\bar{\xi}_{2pt}(r) \equiv \frac{3}{r^3} \int_0^r d\tilde{r} \tilde{r}^2 \xi_{2pt}(\tilde{r}) \quad (10)$$

is its volume average, equation (7) can be cast into a more intuitive form:

$$\frac{\langle \delta(\mathbf{r}) \xi_{ij} \rangle}{\sigma_0} = \frac{\xi_{2pt}(r) - \bar{\xi}_{2pt}(r)}{\sigma_0^2} \hat{r}_i \hat{r}_j + \frac{\bar{\xi}_{2pt}(r)}{3\sigma_0^2} \delta_{ij}. \quad (11)$$

In this expression, one should think of  $\bar{\xi}$  as the overdensity within  $r$ , and  $\bar{\xi} - \xi$  as the difference between the overdensity within  $r$  and that at  $r$  itself.

Inserting this in equation (5) yields

$$\langle \delta(r, \mu) | \Xi \rangle = \langle \delta | \Xi \rangle \Delta_0(r) - 5 \langle \ell | \Xi \rangle \Delta_2(r) P_2(\mu), \quad (12)$$

where  $\mu = \cos \theta$ ,  $P_2(\mu) = (3\mu^2 - 1)/2$  is a Legendre polynomial,

$$\langle \delta | \Xi \rangle \equiv \sigma_0 \langle \xi_{11} + \xi_{22} + \xi_{33} | \Xi \rangle, \quad (13)$$

$$\langle \ell | \Xi \rangle \equiv \sigma_0 \langle \xi_{11} - \frac{\xi_{22} + \xi_{33}}{2} | \Xi \rangle. \quad (14)$$

In this form, it is clear that the first term on the rhs of equation (12),  $\langle \delta | \Xi \rangle \xi_{2pt}(r)/\sigma_0^2$ , is the spherical average of the full expression. Therefore, the prefactor should be thought of as a ‘linear bias factor’

$$b(\Xi) \equiv \langle \delta | \Xi \rangle / \sigma_0^2 \quad (15)$$

coming from the constraints  $\Xi$ . (We provide an explicit example of this in the next section.) The angular dependence comes from the second term, which vanishes when  $\ell = 0$ , i.e., for spherical objects.

Since both  $b(\Xi) \xi_{2pt}(r)$  and its angle average  $b(\Xi) \bar{\xi}_{2pt}(r)$  can be measured (indeed, these are the traditional 2-point measurements), our model can be written as

$$\frac{\langle \delta(r, \mu) | \Xi \rangle}{\langle \delta | \Xi \rangle \Delta_0(r)} = 1 - A(\Xi) \frac{\Delta_2(r)}{\Delta_0(r)} P_2(\mu), \quad (16)$$

where

$$A(\Xi) \equiv 5 \langle \ell | \Xi \rangle / \langle \delta | \Xi \rangle. \quad (17)$$

The left hand side is the ratio of observables, and the right hand side shows that it is the product of a scale-independent amplitude, and a separable function of scale  $r$  and angle. Since the  $r$  dependence is completely specified by measurable angle-averaged quantities, and the  $\mu$  dependence is simply that of a quadrupole, the amplitude is the only free parameter in our model. In this respect, the expression above should be thought of as providing a generic fitting formula with just one free parameter, the amplitude. In our model, this amplitude encodes information about the alignment between the tracer field and the large scale environment.

## 2.3 Illustrative constraints

The averages over  $\Xi$  in equations (13) and (14) can be calculated for many scenarios. To gain intuition, suppose that we

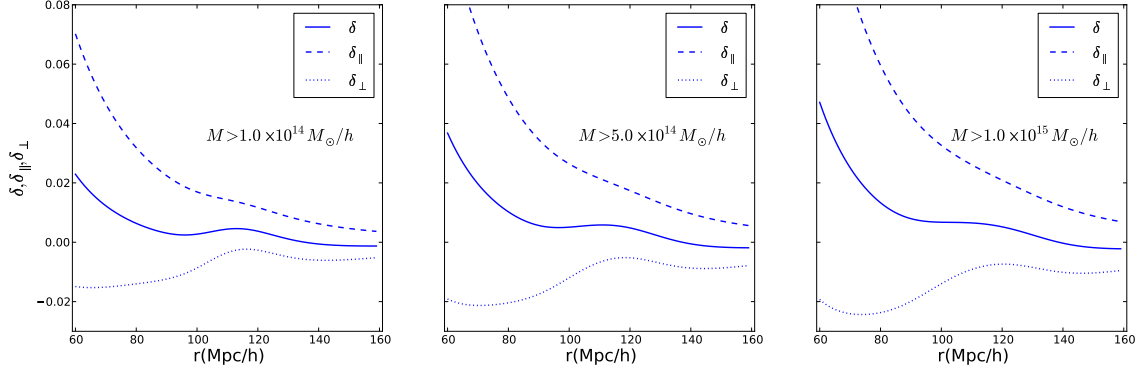


**Figure 1.** Equation (12) with  $\sum_i \xi_{ii} > 1.66/\sigma_0$  and  $\xi_{22,33} > \xi_{11} > 0.41/\sigma_0$  for different mass scales.

identify haloes with regions in the initial field for which all three eigenvalues were positive (e.g. Lee & Shandarin 1998). In this case, requiring

$$\Xi = \{\xi_{33} > \xi_{22} > \xi_{11} > 0\} \quad (18)$$

means that

$$\langle \xi_{11} | \Xi \rangle = \frac{1}{30\sqrt{\pi}P(\Xi)}(\sqrt{15} - \sqrt{10}), \quad (19)$$

$$\langle \xi_{22} | \Xi \rangle = \frac{1}{180\sqrt{\pi}P(\Xi)}(14\sqrt{15} - 13\sqrt{10}), \quad (20)$$

$$\langle \xi_{33} | \Xi \rangle = \frac{1}{180\sqrt{\pi}P(\Xi)}(-5\sqrt{15} + 14\sqrt{10}), \quad (21)$$

where

$$P(\Xi) = \frac{1}{2} - \frac{\arctan(\sqrt{5})}{2\pi} - \frac{\sqrt{5}}{3\pi} \approx \frac{2}{25}. \quad (22)$$

This makes

$$b(\Xi) = \frac{\langle \delta | \Xi \rangle}{\sigma_0^2} = \frac{\sqrt{10}}{72\sqrt{\pi}P(\Xi)} \frac{3\sqrt{6} - 2}{\sigma_0} \approx \frac{5}{3\sigma_0} \quad (23)$$

and  $A(\Xi) \approx -7/4$ . This shows that the bias factor increases as  $\sigma_0$  decreases. We remarked earlier that, in the excursion set approach, large masses have small  $\sigma_0$ . Therefore, this model has the monopole part of the signal increasing as mass increases, but the ratio of the monopole to the quadrupole is independent of halo mass.

## 2.4 More realistic conditions for haloes and voids

Figure 1 shows the result of evaluating equation (12) numerically with  $\Xi$  given by the requirement that  $\sum_i \xi_{ii} > 1.66/\sigma_0$  and  $\xi_{22,33} > \xi_{11} > 0.41/\sigma_0$  for a range of choices of  $\sigma_0$ . These constraints on the  $\xi_{ij}$  were motivated by the spherical collapse model and additional analysis in Lam et al. (2009). The values of  $\sigma_0$  were chosen to match the halo masses quoted by Faltenbacher et al. (2012) in their analysis of the anisotropic clustering around haloes in simulations.

It is encouraging that the amplitude and scale dependence of our predicted signal are qualitatively rather similar to theirs, although our angular dependence is slightly larger than they report. While errors in measuring the direction of the long axis of each halo will weaken the measured signal, thus alleviating some of the discrepancy, there are at least

three other reasons why this may happen. First, our model of the Lagrangian patches which become haloes is crude, and may be inadequate. Second, haloes are not, in fact, perfectly aligned with the shear (e.g. Lee & Pen 2001). And third, our model is based on linear theory; recent work has shown that nonlinear evolution will induce a quadrupole even if none is initially present, and will modify it if there is one initially (Chan et al. 2012, although, on the scales of most interest here, this is expected to be subdominant). Accounting for this will weaken the predicted signal.

Other non-linear structures include filaments, sheets, and voids. In triaxial models, this classification is related to the eigenvalues of the shear (Shen et al. 2006). All positive eigenvalues describe a halo, one negative gives a filament, two negatives a sheet, and all three negative a void (e.g. Hahn et al. 2007). For voids a reasonable set of conditions on the eigenvalues is  $0 > \xi_{22,33} > \xi_{11}$  and  $\sum_i \xi_{ii} < -2.8/\sigma_0$ . Again, the latter condition is from the spherical evolution model (see e.g. Sheth & van de Weygaert 2004). Figure 2 shows the result. In the direction of the major axis, there is a positive boost similarly to the case of haloes. Of course, since voids are driven towards spherical symmetry, their orientation may be harder to measure accurately.

## 2.5 The shear vs the inertia tensor

Haloes have been shown to align with the Lagrangian shear (Dubinski 1992; Lee & Pen 2001), and triaxial collapse models relate halo shapes to the initial shear (Sheth et al. 2001; Lee et al. 2005; Rossi et al. 2011). These findings single out the shear tensor from others that could potentially define the axes of structures. An alternative to the shear is the initial inertia tensor (the matrix of second derivatives of the density field). E.g., in the peaks model of (Bardeen et al. 1986), haloes form at the peaks of the Lagrangian density field so their shape is given by the inertia tensor.

The matter distribution around a peak with conditions on the inertia tensor is given by equation (7.8) of Bardeen et al. (1986). Angle averaging their expression around axis 1 yields

$$\begin{aligned} \frac{\delta(r, \mu)}{\sigma_0} &= \frac{\nu - \gamma x}{1 - \gamma^2} \Delta_0(r) - \frac{\gamma \nu - x}{1 - \gamma^2} \tilde{\Delta}_0(r) \\ &\quad - 5\left(\Lambda_1 - \frac{\Lambda_2 + \Lambda_3}{2}\right) \tilde{\Delta}_2(r) P_2(\mu), \end{aligned} \quad (24)$$

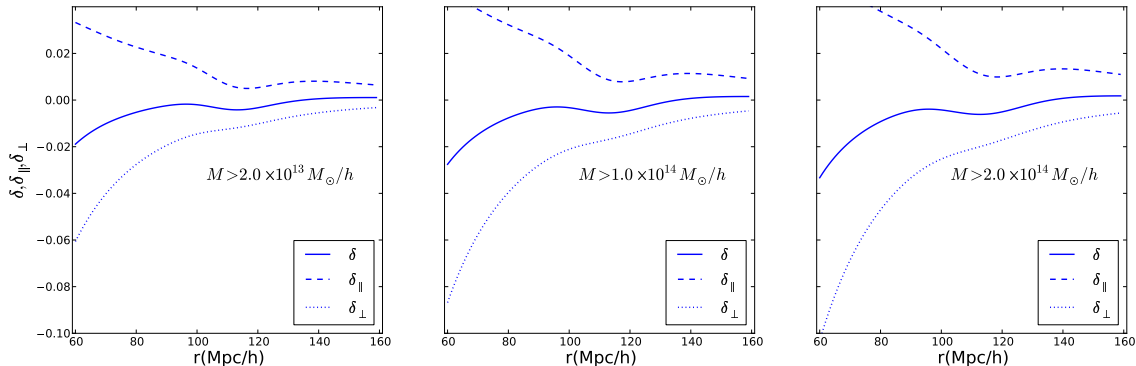


**Figure 2.** The same as Figure 1 but with  $\sum_i \xi_{ii} < -2.8/\sigma_0$  and  $0 > \xi_{22,33} > \xi_{11}$ .

where  $\Lambda_1, \Lambda_2$  and  $\Lambda_3$  are the eigenvalues of  $-\partial^2 \delta(0)/\partial q_i \partial q_j$ ,  $x = \sum_i \Lambda_i$ ,  $\nu = \delta/\sigma_0$ ,  $\gamma = \sigma_1^2/(\sigma_0 \sigma_2)$ , and

$$\tilde{\Delta}_n(r) \equiv \frac{1}{2\pi^2 \sigma_0 \sigma_2} \int dk k^4 j_n(rk) W_R(k) P(k). \quad (25)$$

It is worth noting that  $\Lambda_1 - (\Lambda_2 + \Lambda_3)/2$  is  $(3y + z)/2$ , where  $y$  and  $z$  are the anisotropy parameters of Bardeen et al. (1986).

Although we have yet to average over the  $\Lambda_i$ , comparison with equation (12) shows that the first two terms in equation (24) will yield the monopole, and the final term a quadrupole. Although the quadrupole here depends on the eigenvalues  $\Lambda$  of the inertia tensor in the same way that the quadrupole in equation (12) depends on the eigenvalues of the shear tensor, we might expect the amplitude here will be much smaller. This is because the integral which defines  $\tilde{\Delta}_2$  has two additional powers of  $k$  compared to that which defines  $\Delta_2$ . However, we must also check that the average over the  $\Lambda_i$  does not yield a large amplitude to compensate for this difference.

To see that this will not happen, note that on large scales, the leading order contribution to the monopole is given by the first term on the rhs of equation (24). With the peak constraints, the quantity  $\tilde{\nu} \equiv (\nu - \gamma x)/(1 - \gamma^2)$  is a Gaussian variate, and it is independent of the  $\Lambda_i$ . This means that we can choose the constraints on  $\tilde{\nu}$  to match the monopole of equation (12), leaving us to perform an independent average over the distribution of parameters  $x$ ,  $y$ , and  $z$  (e.g. Appendix C of Bardeen et al. 1986). The resulting angular dependence is so weak that it cannot be distinguished from the solid curve shown in Figure 1. Since the nonlinear evolution effects described by Chan et al. (2012) cannot, on their own, account for the signal seen by Faltenbacher et al. (2012), we conclude that the initial shear tensor matters for the angular dependence, whereas the inertia tensor does not.

### 3 DISCUSSION

In this paper, we calculated the anisotropy in the linear density field when conditions are placed on the Lagrangian shear field. If the shear field is strongly correlated with the shapes and orientations of nonlinear haloes, then this calculation should be closely related to the anisotropy of the halo-mass

cross-correlation function, which is most easily seen when the mass field around haloes is stacked after aligning along the major axis of the halo (e.g. Faltenbacher et al. 2012).

For haloes, our model (equation 12) captures the main features of the cross-correlation function measurement. The signal along the long axis is stronger than perpendicular to it, but produces a less prominent BAO feature (Figure 1). We predict a similar effect for voids (Figure 2). The overall amplitude of the effect is slightly stronger in our model than in the simulations. This may be due to inadequacies in our crude model which relates halo formation to the local shear; it may arise because the alignment between haloes and the shear is not perfect; or nonlinear evolution may have had a small effect (see Section 2.4). We also argued that the measured amplitude is inconsistent with a model in which the alignment is produced by the initial inertia rather than shear tensor (Section 2.5).

Absent a model for halo or void formation, our equation (12) may be treated as a one-parameter family which, given the spherically averaged measurement describes the anisotropy. This parameter depends only on the local shear, and so may be used to constrain models of halo formation and alignment. Further work can be done to incorporate redshift distortions and nonlinearities into the model. Also, tests on simulations are needed in order to identify systematics that can affect the validity of the model. Finally, we are in the process of checking if this sort of measurement can yield useful constraints on modified gravity models.

### 4 ACKNOWLEDGMENT

PP is grateful for a CEI fellowship. RKS was supported in part by NSF 0908241 and NASA NNX11A125G. He is grateful to B. Bassett for organizing a mini-workshop at AIMS in January 2012 where he had interesting discussions with A. Faltenbacher and U.-L. Pen about this effect, as well as the participants of the Cape Town Cosmology School 2012 for inspiration. He is also grateful to the group at LUTH in Meudon Observatory for their hospitality during June 2012.

## REFERENCES

- Bardeen J. M., Bond J. R., Kaiser N., Szalay A. S., 1986, ApJ, 304, 15
- Bond J. R., Cole S., Efstathiou G., Kaiser N., 1991, ApJ, 379, 440
- Bond J. R., Myers S. T., 1996, ApJS, 103, 1
- Chan K. C., Scoccimarro R., Sheth R. K., 2012, Phys. Rev. D, 85, 083509
- Desjacques V., 2008, MNRAS, 388, 638
- Doroshkevich A. G., 1970, Astrophysics, 6, 320
- Dubinski J., 1992, The Astrophysical Journal, 401, 441
- Eisenstein D., 2005, New Astronomy Reviews, 49, 360
- Faltenbacher A., Li C., Wang J., 2012, ApJ, 751, L2
- Hahn O., Carollo C. M., Porciani C., Dekel A., 2007, MNRAS, 381, 41
- Jones B. J. T., van de Weygaert R., Aragón-Calvo M. A., 2010, MNRAS, 408, 897
- Kaiser N., 1987, MNRAS, 227, 1
- Lam T. Y., Sheth R. K., Desjacques V., 2009, MNRAS, 399, 1482
- Lee J., Jing Y. P., Suto Y., 2005, ApJ, 632, 706
- Lee J., Pen U.-L., 2001, ApJ, 555, 106
- Lee J., Shandarin S. F., 1998, ApJ, 500, 14
- Lewis A., Challinor A., Lasenby A., 2000, Astrophys. J., 538, 473
- Peebles P., 1980, The large-scale structure of the universe. Princeton Univ Pr
- Press W. H., Schechter P., 1974, ApJ, 187, 425
- Rossi G., Sheth R. K., Tormen G., 2011, MNRAS, 416, 248
- Schlagenhauser H. A., Phleps S., Sanchez A. G., 2012, ArXiv e-prints
- Shen J., Abel T., Mo H. J., Sheth R. K., 2006, ApJ, 645, 783
- Sheth R., Mo H., Tormen G., 2001, Monthly Notices of the Royal Astronomical Society, 323, 1
- Sheth R. K., Tormen G., 2002, MNRAS, 329, 61
- Sheth R. K., van de Weygaert R., 2004, MNRAS, 350, 517
- Smargon A., Mandelbaum R., Bahcall N., Niederste-Ostholt M., 2012, MNRAS, 423, 856